Reflection Shearography for Non-Destructive Evaluation

Russell M. Kurtz[*], Michael A. Piliavin, Ranjit D. Pradhan, Tin M. Aye, Gajendra D. Savant, and
Tomasz P. Jannson

Physical Optics Corporation, Torrance, CA 90501

Steffen Hergert

University of Stuttgart, Stuttgart, Germany

ABSTRACT

Conventional nondestructive evaluation (NDE) techniques include visual inspection, eddy current scanning, ultrasonics, and fluorescent dye penetration. These techniques are limited to local evaluation, often miss small buried defects, and are useful on polished surfaces only. Advanced NDE techniques include laser ultrasonics, holographic interferometry, structural integrity monitoring, shearography, and thermography. A variation of shearography, employing reflective shearographic interferometry, has been developed. This new shearographic interferometer is presented, together with models to optimize its performance and experiments demonstrating its use in NDE.

1. INTRODUCTION

Engineering structures such as engines, nuclear reactors, automotive engines, piping and pressure vessels, and building support structures inherently have stresses, usually produced by material processing or joining operations (welding, rolling, etc.) or during use. Some types of stresses, such as high cycle fatigue (HCF) and fretting fatigue in aircraft engines, can cause fatal crashes[1]. The current techniques for nondestructive testing and evaluation (NDE) of aircraft on-wing components and many other aircraft structures require disassembling these systems and subsystems. These procedures are labor and time intensive, requiring high budgets for maintenance and operation and support (O&S) plus a long period of downtime for testing. Conventional NDE techniques for detecting structural and surface damage include visual inspection, eddy current scanning, ultrasonics, and fluorescent dye penetration[2]. These techniques are limited to *local evaluation*, and often miss small, buried defects. Advanced NDE techniques, including laser ultrasonics[3], digital holographic interferometry[4], shearography[5,6], and thermography[7] can be applied for real-time, high-resolution inspection. However, their usefulness is limited by their bulkiness, sensitivity to external vibrations – and by their low dynamic range, measurement sensitivity, and spatial resolution. We present a technology founded on the principles of shearographic interferometry, employing the shearing element in the reflective mode.

2. THEORY

NDE by reflective shearography depends on three areas: applications of shearography to NDE, detailed analysis of the shearing element, and image processing.

2.1. Shearography for NDE

Shearography is a type of interferometry in which the two interfering wavefronts are virtually identical except for a slight difference in their angle of propagation (the shear angle). For reflective shearography, the shear is induced by reflection from a wedge (Figure 1). The beam with intensity I_2, then, has a slightly different angle (which can appear as a position-dependent phase shift) and a slight position shift with respect to the beam with intensity I_1. If the wedge angle is designed to shift the beam only in the x-direction, the interference between these two beams can be written

[*]Now at RAN Science & Technology, LLC, russell.kurtz@ranscitech.com, phone 1 310 265-4448, fax 1 310 265-4449, http://www.ranscitech.com
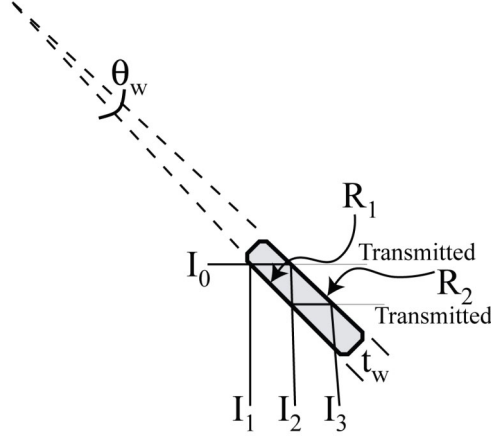
Fig. 1. Layout and parameters of wedge used for reflective shearography.

$$\Gamma_{ref}(x,y) = I_1(x,y) + I_2(x+\Delta x,y) + 2\sqrt{I_1(x,y)I_2(x+\Delta x,y)}\,\cos[\varphi(x,y) - \varphi(x+\Delta x,y) - 2\pi f_0 x]\quad, \qquad (1)$$

where $f_0 = \sin\theta_s/\lambda$, θ_s is the shear angle between the two beams, and λ is the wavelength of the illumination laser. Eq. (1) represents an interference pattern varying in the x-direction with fringe spacing $1/f_0$.

Shearography depends on the difference between two interferograms, one take under reference conditions and the other when stress is applied to the target. This stress affects the phase of the light reflected from the target to the wedge. So the interference pattern under stressed conditions is

$$\Gamma_{stress}(x,y) = I_1(x,y) + I_2(x+\Delta x,y) + 2\sqrt{I_1(x,y)I_2(x+\Delta x,y)}\,\cos[\varphi'(x,y) - \varphi'(x+\Delta x,y) - 2\pi f_0 x]\quad, \qquad (2)$$

where the primed phases indicate that the measurements are taken in the stressed condition. The patterns of Eqs. (1) and (2) are captured and digitized, so that the difference image (a "shearogram" – the difference image between two shearographic interferograms) can be created. This image's overall intensity is

$$\Delta\Gamma(x,y) = \Gamma_{stress}(x,y) - \Gamma_{ref}(x,y) = 4\sqrt{I_1 I_2}\,\sin\!\left(\frac{\varphi_+(x,y)}{2}\right)\sin\!\left(\frac{\varphi_-(x,y)}{2}\right), \qquad (3)$$

where φ_+ is the sum of the phases of the stressed and reference interferograms and φ_- is their difference. The sum term includes $\sin(4\pi f_0 x)$, and is a rapidly-varying term that effective adds to the speckle noise, but the difference term is

$$\varphi_-(x,y) = [\varphi'(x,y) - \varphi(x,y)] - [\varphi'(x+\Delta x,y) - \varphi(x+\Delta x,y)]\quad. \qquad (4)$$

This includes the useful term

$$\delta \equiv \varphi'(x,y) - \varphi(x,y) = \frac{2\pi}{\lambda}\mathbf{u}\cdot\mathbf{K}\quad, \qquad (5)$$

where $\mathbf{u}$ is the displacement vector and $\mathbf{K}$ is the sensitivity vector of the shearographic measurement. For the case described above, with shear in the x-direction, we also have

$$\delta = \delta_x = \left(\frac{\partial u}{\partial x}k_s e_x + \frac{\partial v}{\partial x}k_s e_y + \frac{\partial w}{\partial x}k_s e_z\right)\Delta x\quad, \qquad (6)$$

where u, v, and w are the components of the displacement vector in the x, y, and z directions, respectively, and e_x, e_y, and e_z are the direction cosines of $\mathbf{K}$. Thus, the result described by eq. (3), over distances much larger than $1/f_0$, is the gradient of the deformation. The gradient of the deformation also defines the strain tensor, so shearography can be used to measure stress-induced strain. Additionally, eq. (4) tells us that the large (spacing $\gg 1/f_0$) fringes visible in a shearogram line up along the gradient of the strain tensor, providing a very sensitive measurement of surface strain,

whether caused by surface or subsurface defects. The shearogram can also provide a quantitative measurement of strain with image processing, as described in Section 2.3.

2.2. The shearing element

For reflection shearography, the shearing element is a wedge as shown in Fig. 1. This wedge has the following characteristics: thickness t_w, front- and rear-surface reflectivities R_1 and R_2 respectively, wedge angle θ_w, and refractive index n_w (we assume it is non-absorbing). For near-normal incidence, the shear angle between the first- and second-surface reflections is

$$\theta_s = 2\theta_w + \sin^{-1}\left\{ n_w \sin\left[\theta_w - 2\sin^{-1}\left(\frac{\sin\theta_w}{n_w} \right) \right] \right\} \quad . \tag{7}$$

This value enables calculation of the spacing between interference fringes in the surface reflection. For digital shearography, the fringe pattern must be visible, indicating that the spacing between fringes must be several pixels. This is complicated by the speckle introduced when a scattering surface (typical of targets of interest) is illuminated by a laser (generally needed for interferometry). There must be at least two complete fringe cycles in every speckle. Thus, the speckle size is controlled as well as the spacing between fringes. The average speckle diameter is

$$d_s = M \frac{\lambda x}{D_a} \quad , \tag{8}$$

where D_a is the diameter of an aperture placed in the expanding beam a distance x from the wedge, λ is the illumination wavelength, and M is the image magnification of any optics between the aperture and the wedge. Due to the random nature of speckle, it is generally prudent to design the speckle size to be at least three times the interferometric fringe spacing.

For near-normal incidence, the image shift due to shear is

$$\Delta x = \frac{2t_w}{n} \frac{\sin\theta_w}{\sqrt{1 - \sin^2\theta_w / n^2}} \approx \frac{2t_w}{n}\theta_w \tag{9}$$

for small wedge angles. For wedge angles typically used in reflection shearography, this is less than the fringe spacing.

The reflectivity of the front and rear surfaces must be optimized. To do so, we refer again to Fig. 1. All useful information is contained in the interference pattern formed by the beams whose intensities are I_1 and I_2. It is easy to calculate their intensities:

$$I_1 = R_1 I_0 \tag{10}$$

and

$$I_2 = R_2\left[1 + 6R_1 + R_1^2 - 4\sqrt{R_1}\left(1 + R_1\right) \right]I_0 \quad . \tag{11}$$

All other reflections show up as noise:

$$I_{noise} \equiv \sum_{i=3}^{\infty} I_i = \frac{R_1 R_2^2}{1 - R_1 R_2}\left[1 + 6R_1 + R_1^2 - 4\sqrt{R_1}\left(1 + R_1\right) \right]I_0 \quad . \tag{12}$$

The interferometric fringe contrast is

$$C_F = \frac{I_{max} - I_{min}}{I_{max} + I_{min}} \quad , \tag{13}$$

where I_{max} and I_{min} are the maximum and minimum intensities, respectively, in the interference pattern. If noise is neglected, $I_{max} = I_1 + I_2$ and $I_{min} = I_1 - I_2$, so the contrast is optimized for $I_1 = I_2$. The brightest reflection that satisfies

this condition obtains when $R_1 = 38.1\%$ and $R_2 = 100\%$. Unfortunately, these reflectivities result in unacceptably high noise ($\sim 25\%$ of the maximum signal). When noise is included, $I_{max} = I_1 + I_2 - I_{noise}$ and $I_{min} = I_1 - I_2 + I_{noise}$. Since the peak value of the *useful* signal is $I_1 + I_2$, we can define a signal-to-noise ratio as

$$ SNR \equiv \frac{I_1 + I_2}{I_{noise}} = \frac{1}{R_1 R_2} + \frac{1}{R_2^2 \left(1 - \sqrt{R_1}\right)^2} \quad . \tag{14}$$

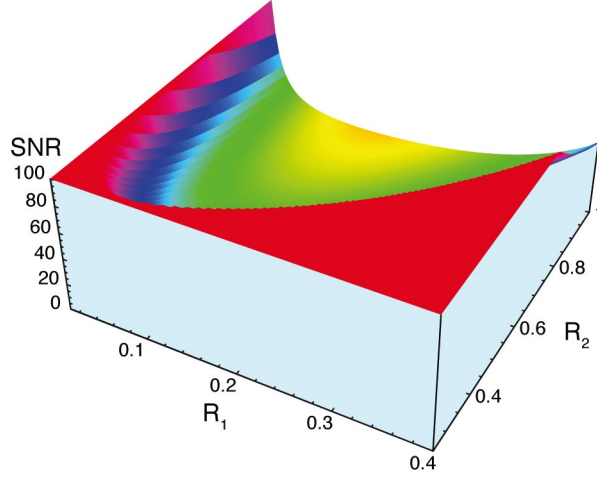This equation is plotted in Fig. 2.

Fig. 2. Shearographic signal-to-noise ratio as a function of front- and rear-surface wedge reflectivity (R_1 and R_2, respectively). For visibility, SNR was clipped at 100.

SNR is large for low reflectivities, since I_{noise} contains an extra factor of $R_1 R_2$ compared to I_2. But at low reflectivities little of the light reaching the wedge is reflected to the detector, reducing or even eliminating any capability of measuring the interferometric signal. The peak reflectivity, the brightest signal reflected (at a point of constructive interference) divided by the incoming intensity, is

$$ R_{eff} \equiv \frac{I_{sig}}{I_0} = R_1 + R_2 \left(1 - \sqrt{R_1}\right)^4 + 2\sqrt{R_1 R_2 \left(1 - \sqrt{R_1}\right)^4} \quad . \tag{15}$$

In eq. (15), I_{sig} is the maximum signal intensity ($I_{max} - I_{noise}$). Effective reflectivity is greatest for high front surface reflectivity R_1, although low values of R_1 can result in high effective reflectivity if R_2 is large. This is shown in Fig. 3.
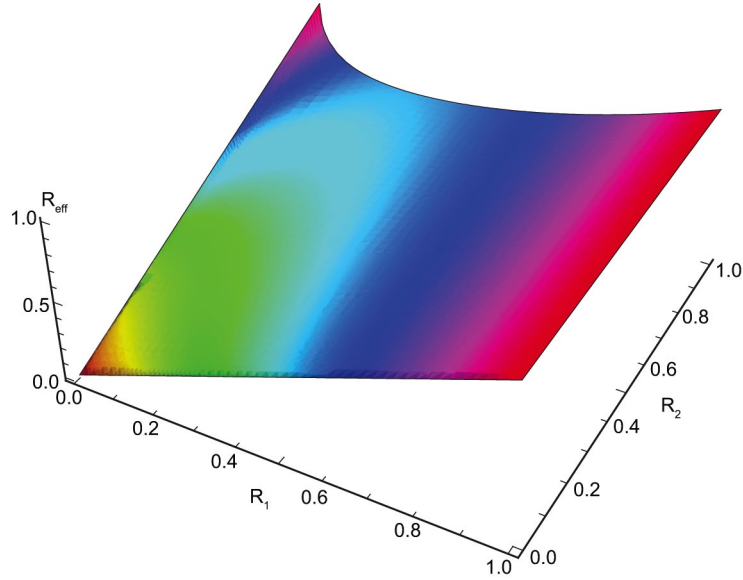
Fig. 3. Effective wedge reflectivity as a function of front- and rear-surface reflectivities.

Since the SNR can, theoretically, reach ∞, a more useful measurement is the contrast. This is defined by eq. (13), with the values of I_{max} and I_{min} that include noise. Just as the peak reflectivity is constrained to $0 < R_{eff} < 1$, contrast must be between 0 and 1. The contrast of the shearographic interference pattern, including noise, is

$$C_{EFF} = \frac{4\sqrt{R_1 R_2 \left(1 - \sqrt{R_1}\right)^4} - R_1 R_2^2 \left(1 - \sqrt{R_1}\right)^4}{2\left[R_1 + R_2 \left(1 - \sqrt{R_1}\right)^4\right] + R_1 R_2^2 \left(1 - \sqrt{R_1}\right)^4} \quad . \tag{16}$$

As shown in Fig. 4, the contrast has similar dependence on R_1 and R_2 as the SNR at low R_1, but is reduced at high R_1. This is due to the reduction in I_{max} and increase in I_{min} caused by the noise.
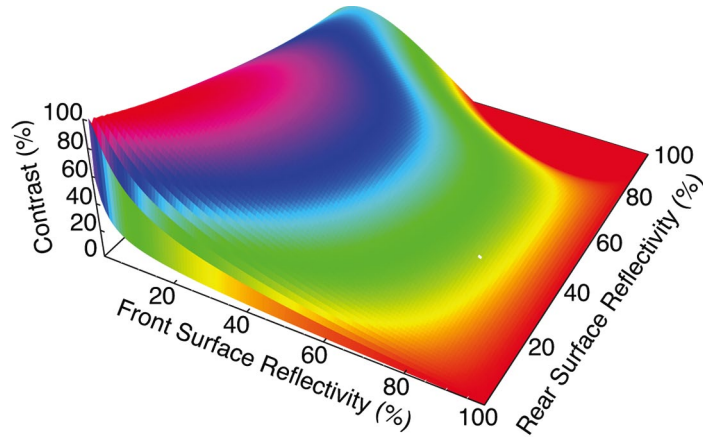

Fig. 4. Interferometric fringe contrast, including effects of noise, as a function of front- and rear-surface wedge reflectivities.

Since a shearographic system requires good contrast, but also needs a large signal (or high peak reflectivity), a figure of merit that is the product of these two factors is a good starting point for design of a reflecting shearographic wedge. The figure of merit is

$$\text{FOM} \equiv R_{\text{eff}}C_{\text{EFF}} = \frac{\sqrt{R_1 R_2}\left[R_1 - \sqrt{R_1} + \sqrt{R_1}\left(1-\sqrt{R_1}\right)^2\right]^2\left[4 - R_2\sqrt{R_1 R_2}\left(1-\sqrt{R_1}\right)^2\right]}{2R_1 + 2R_2\left(1-\sqrt{R_1}\right)^4 + R_1 R_2^2\left(1-\sqrt{R_1}\right)^4} \quad . \tag{17}$$

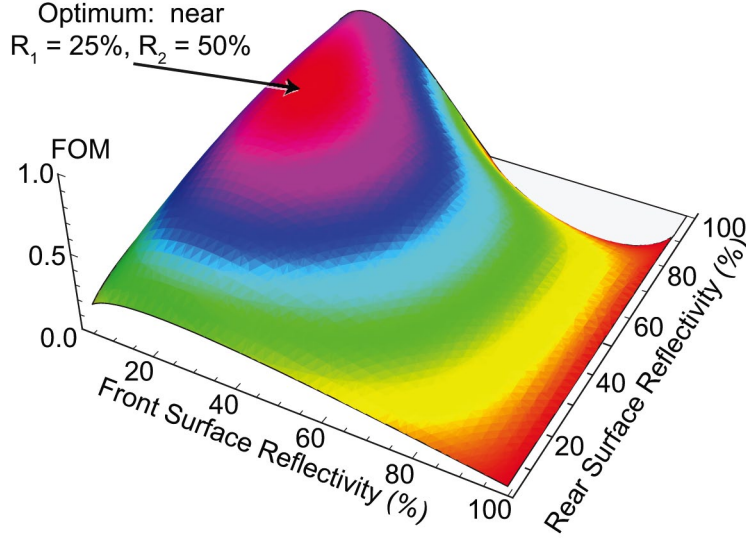The wedge design figure of merit is presented in Fig. 5.

Fig. 5. Wedge design figure of merit.

2.3. Image processing to quantify strain

It is possible to detect phase differences in the shearographic signal through the use of Fourier transforms[8]. To do so, eq. (1) is first rewritten in terms of the electric field instead of the intensity:

$$\Gamma(x,y) = u_1(x,y)u_1^*(x,y) + u_2(x+\Delta x,y)u_2^*(x+\Delta x,y) + u_1(x,y)u_2^*(x+\Delta x,y) + u_2(x+\Delta x,y)u_1^*(x,y) , \tag{18}$$

where u_j is the electric field of wave j, u^* is the complex conjugate of u, and the intensity at each point is

$$I_j = u_j u_j^* \quad . \tag{19}$$

We take the Fourier transform of Eq. (18), which converts it from the space domain to the spatial frequency domain,

$$\Im(\Gamma) = U_1 \otimes U_1^* + U_2 \otimes U_2^* + U_1 \otimes U_2^* + U_2 \otimes U_1^* , \tag{20}$$

where the convolution operator $\otimes$ has replaced multiplication because multiplication in the space domain is convolution in the spatial frequency domain, and U_j is the Fourier transform of u_j.

In a real system, the signal of eq. (18) is captured by a CCD camera, resulting in a digitzed signal. This is then Fourier transformed by the fast Fourier transform routine, FFT. The first two convolution terms in eq. (20) are centered on zero frequency, while the cross terms, which contain the phase information, are complex conjugates of each other. The computer applies a mask to select only the first cross term and set the others to zero. The inverse Fourier transform then yields

$$\Im^{-1}\left(U_1 \otimes U_2^*\right) = u_1(x,y)u_2^*(x,y) \quad , \tag{21}$$

which is a complex function. Then, from Eqs. (1), (4), and (18) we find

$$\varphi(x,y) - \varphi(x + \Delta x, y) - 2\pi \, x \, f_0 = \tan^{-1}\left(\frac{\text{Im}\left[u_1(x,y)u_2^*(x,y)\right]}{\text{Re}\left[u_1(x,y)u_2^*(x,y)\right]}\right), \tag{22}$$

where Im[ ] is the imaginary part and Re[ ] is the real part. A similar equation obtains for the deformed shearogram, and the strain related phase change $\varphi\_(x,y)$ can be calculated easily. The magnitude of the strain gradient can then be calculated from eq. (6).

3. EXPERIMENT

We performed an experiment to demonstrate the use of reflection shearography in NDE. A thin piece of aluminum with a scratch on the back was placed in a holder and tested. Stress was applied by heating the aluminum with a CO_2 laser. The unstressed image and its associated phase are shown in Fig. 6.

(a)   (b)
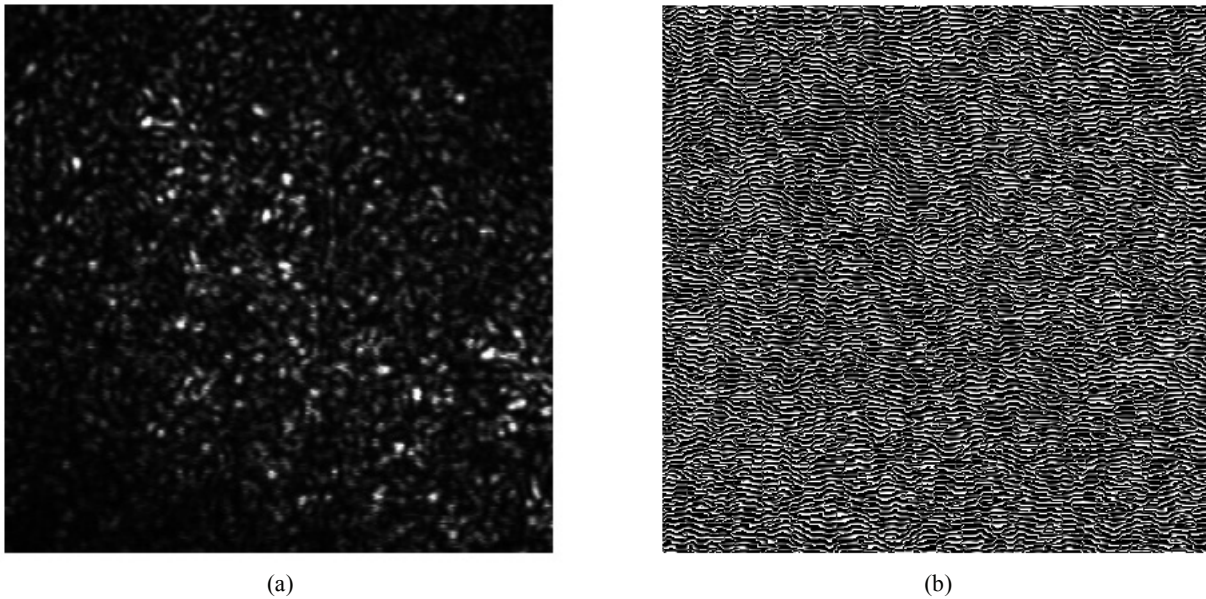
Fig. 6. Speckle pattern from illuminated area (a) and wrapped phase (b) for an unstressed aluminum plate.

The interference pattern is visible within the speckles in Fig. 6(a). There was no visible difference in the speckle pattern or the wrapped phase between the stressed and unstressed images. In each case, the phase was calculated by the Fourier transform method described in Section 2.3. This process appears in Fig. 7.

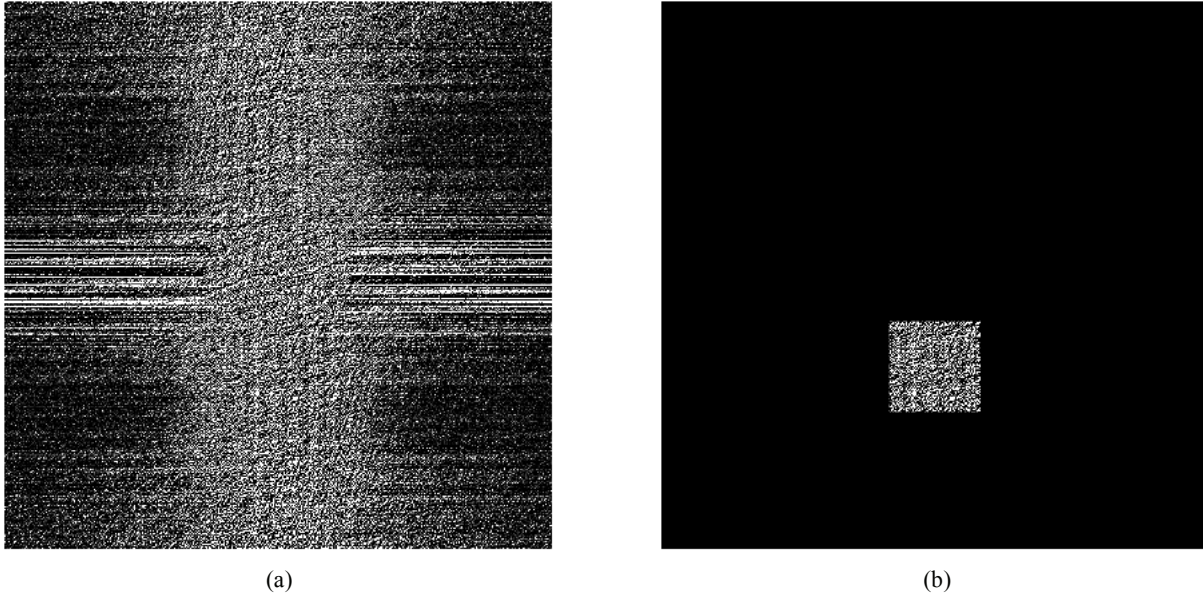(a)   (b)

Fig. 7. The Fourier transform method of calculating phase. First, the image (Fig. 6(a)) is transformed (a). Then the area of interest, offset from the center by the fringe frequency f_0, is selected (b). When this selection is inverse transformed, the argument of the resulting complex array is the "wrapped" phase – the phase modulo 2π (Fig. 6(b)).

After obtaining the phase of the images taken under reference and stressed conditions, the derivative of the strain tensor can be determined. It is the difference between the phases of these images (eqs. (5) and (6)). The unwrapped phase (continuous, without the 2π jumps) looks the same in the stressed and unstressed cases, but the difference shows a stress location near the bottom of the image (Fig. 8).

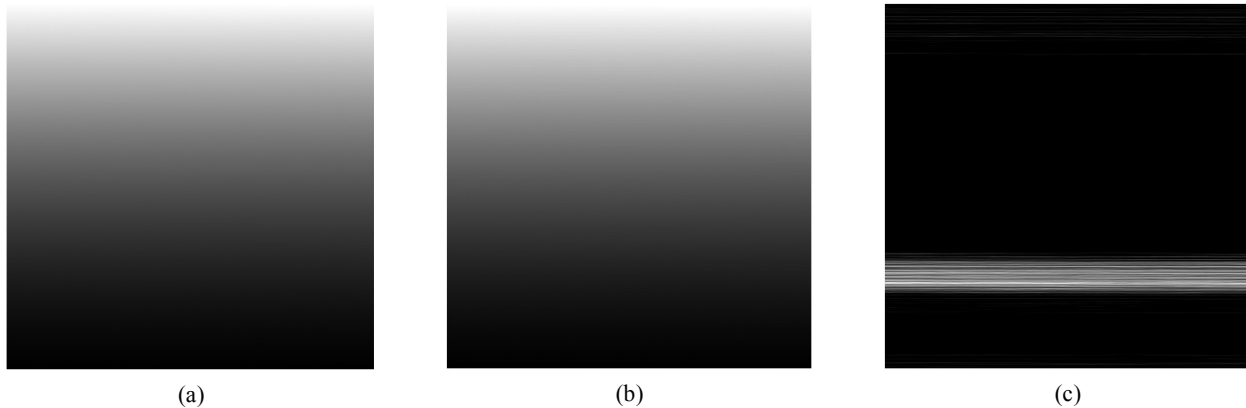(a)   (b)   (c)

Fig. 8. Determining location of stress. The difference between the two phase images, (a) reference and (b) stressed object, is taken. This difference (c) represents the derivative of the strain tensor.

4. CONCLUSIONS

Reflection shearography has been shown to be a useful technique for measuring strain in objects. It relies on applying stress to an object and determining the difference between the phase of the reflected light in the unstressed (reference) and stressed cases. This method is capable not only of qualitatively locating stress, but also of quantifying the gradient of the strain tensor for the object under test.

REFERENCES

1. J. Deutch, *AFOSR Workshop on Jet Engine High Cycle Fatigue*, 1995.
2. P.K. Sharp, D.E. Rowlands, and G. Clark, "Evaluation of Innovative NDI Methods for Detection of Widespread Fatigue Damage*," Defence Sceience and Technology Organization, Australia*, 1996.
3. A.D. McKie and R.C. Addison Jr., "Laser-Based Ultrasonic Inspection of Complexly Contoured Composite and Metallic Structures for Aerospace Applications," *SPIE Nondestructive Evaluation of Aging Aircraft, Airports, and Aerospace Hardware*, vol. 3397, 107-116, 1998.
4. H. Fein, "Holographic Analysis of the Structural and Operational Dynamics of an Advanced Graphite-Epoxy Composite Flight Control Structure," *SPIE Nondestructive Evaluation of Aging Aircraft, Airports, and Aerospace Hardware*, vol. 3397, 179-188, 1998.
5. J.W. Newman, "Shearographic Inspection of Aircraft Structure*," Mater. Eval.*, **49**, 1106-1109, 1991.
6. W.J. Bisle, D. Scherling, and G. Tober, "Phase Stepping Shearography for Testing Commercial Aircraft Structure: An Application Review of Advanced Image Processing Techniques for Shearography," *Rev. Prog. Quant.*, D. Thompson and D.E. Chimenti, Vol. 15, Plenum Press, New York, 1996.
7. J. Prati, "Detecting Hidden Exfoliation Corrosion in Aircraft Wing Skins Using Thermography," *SPIE Thermosense*, vol. 4020, 200-209, Orlando, Florida, 2000.
8. G. Pedrini, Y.L. Zou, and H.J. Tiziani, "Quantitative Evaluation of Digital Shearing Interferogram Using the Spatial Carrier Method*," Pure Appl. Opt.*, **5**, 313-321, 1996.